NOLTR 63-73

# THE COMPRESSIBILITY OF PYROLYTIC GRAPHITE



22 MAY 1963

NOL
UNITED STATES NAVAL ORDNANCE LABORATORY, WHITE OAK, MARYLAND

# THE COMPRESSIBILITY OF PYROLYTIC GRAPHITE

By: N. L. Coleburn

ABSTRACT: The compressibility of pyrolytic graphite has been dynamically measured at pressures up to 0.5 megabar by utilizing explosive-generated shock waves. Shock and free-surface velocities normal and parallel to the original plane of graphite deposition were measured optically. The Rankine-Hugoniot shock wave equations were used to determine the compression points corresponding to the measured velocities. The measurements failed to distinguish statistically between the two major crystal directions in regard to dynamic compressibility characteristics.

The measured pressure-volume data for pyrolytic graphite and the results of Alder and Christian on natural graphite differ significantly at pressures above 100 kilobars. Within the range of the present experiments no transition of pyrolytic graphite to diamond was found.

PUBLISHED SEPTEMBER 1963

EXPLOSION DYNAMICS DIVISION
EXPLOSIONS RESEARCH DEPARTMENT
U. S. NAVAL ORDNANCE LABORATORY
WHITE OAK, MARYLAND

NOLTR 63-73 22 May 1963

The Compressibility of Pyrolytic Graphite

This work was done in the Explosion Dynamics Division, Explosions Research Department under Bureau of Naval Weapons (SP) Resource Category #WW0041, PR-14. An important aspect of this task is research on the properties of possible re-entry body materials. The work of this report is a contribution to this particular aspect of the task.

It is a pleasure to acknowledge the co-operation of Bernard E. Drimmer and Thomas P. Liddiard, Jr. in several of the low pressure shock measurements, and Howard T. Savage in the sound velocity measurements. The author is especially indebted to William A. Brown for his valuable assistance in carrying out the experimentation.

R. E. ODENING
Captain, USN
Commander

C. J. ARONSON
By direction

CONTENTS


| | | Page |
|---|---|---|
| I. | INTRODUCTION | 1 |
| II. | EXPERIMENTAL METHOD | 1 |
| III. | EXPERIMENTAL ASSEMBLIES | 2 |
| IV. | RESULTS | 12 |
| V. | DISCUSSION | 12 |
| VI. | REFERENCES | 20 |


TABLES


| Table | Title | Page |
|---|---|---|
| 1 | Explosive-Generated Shock Systems and Calibration Parameters | 6 |
| 2 | Summary of Shock Wave Measurements Along A and C Axes | 10 |
| 3 | Rankine-Hugoniot Shock Wave Parameters of Pyrolytic Graphite | 13 |
| 4 | Longitudinal Sound Velocity | 14 |
| 5 | Calculated Rankine-Hugoniot Temperatures and 25°C Isotherm for the Compression of Pyrolytic Graphite | 19 |


ILLUSTRATIONS


| Figure | Title | Page |
|---|---|---|
| 1 | Experimental Arrangement for Delivery of a Plane Shock Wave to the Test Specimens | 3 |
| 2 | Arrangement for Obtaining Pressure of 0.3-1.0 megabar | 4 |
| 3 | Specimen Plate Arrangement | 7 |
| 4 | Two-slit Smear Camera Record of Shock Wave Arrivals on the Free Surfaces of the Test Specimens and Aluminum Specimen Plate, and Free-Surface Arrivals at the Glass Witness Plate | 8 |
| 5 | Shock Velocity ($U_s$) - Particle Velocity ($U_p$) Curve for Pyrolytic Graphite | 11 |
| 6 | The Compressibility of Graphite | 15 |
| 7 | Compressibility vs Relative Volume of Pyrolytic Graphite | 16 |

## I. INTRODUCTION

In late 1961, Alder and Christian[1] reported pressure-volume data for natural Ceylon graphite which had been compressed up to 0.8 megabars by shock waves. The authors interpreted their measurements as showing the direct transformation of graphite to diamond in the range of 0.3 to 0.4 megabar. Earlier in 1961, De Carli and Jamieson[2] had recovered small diamonds by the transformation of artificial graphite shocked to 0.3 megabar but were unable to obtain this conversion by shocking pure hexagonal graphite. They proposed that structural differences in the graphite accounted for the different results. In reference to these results the various forms of graphite are known to have dissimilar physical and chemical properties. However the compressibility of pure hexagonal graphite as a function of pressure has not been established, primarily because significant differences have not been expected in the compressibility of the various graphites and pure samples of hexagonal graphite are not easily obtained.

Recent studies[3,4,5] of more readily available pyrolytic graphite have shown that this material has the layer-like properties of pure hexagonal graphite, i.e., passes heat much more readily in one direction than in another, has anisotropies of sound velocity and anisotropies in normal modes of lattice vibration. Further concerted efforts are being made to evaluate other properties of pyrolytic graphite because of its possible use as a re-entry body material. This paper reports the dynamic compressibility of pyrolytic graphite at pressures up to 0.5 megabar. These pressures were obtained from explosive-generated shock waves. The compressibility was determined from the dynamic pressure-volume curve, i.e., the shock Hugoniot, using optical measurements of the shock wave and particle velocity as a function of orientation (the shock wave propagation was directed parallel and perpendicular to the C-axis). The pressure-volume data have been compared to the dynamic measurements of Alder and Christian and the static data of Bridgman[6] and Vereschagin[7] on natural graphite.

## II. EXPERIMENTAL METHOD

Compressibility data were obtained from shock wave experiments by relating the measured velocities, $U_s$, of the shock wave, and $u_p$, of material behind the shock front to the pressure, P, and specific volume, V, of the compressed material. The relationships are given by the Rankine-Hugoniot equations expressing conservation of mass and momentum:

$$\frac{V}{V_o} = (U_s - u_p)/(U_s - u_o)$$

$$P-P_o = \frac{1}{V_o} (U-u_o) (u_p-u_o) \qquad (2)$$

(The subscript, o, refers to conditions in the undisturbed region immediately ahead of the shock front.) While the shock wave velocity may be measured directly, the particle velocity is determined indirectly by measuring the free-surface motion of the shocked specimen. Motion of the free surface is produced by reflection of the shock wave as a rarefaction wave at the free surface. The free surface acquires a velocity, $u_f$, which for a plane shock wave is almost identically twice the particle velocity of the shocked material [8,9],

$$u_f \doteq 2u_p \quad . \qquad (3)$$

The particle velocity can be determined also from the method of impedance-matching[10], i.e., by shock-loading the specimen with a standard material whose equation of state is known, and measuring the shock velocity in the specimen. Particle velocities of pyrolytic graphite were determined by both methods.

## III. EXPERIMENTAL ASSEMBLIES

The experimental arrangement which was used is shown in Figs. 1 and 2. The explosive system, a shock driver or attenuating system, the specimen plate, and test specimens, 0.3-cm to 0.9-cm thick, were arranged in sequence. A glass witness plate mounted 0.2 cm from the specimens provided a fixed station for free-surface velocity measurements. The explosive system used a 15.8-cm diameter, plane wave lens[11] to ensure a shock wave free of side rarefactions within the region of measurement. This lens produced a shock wave which emerging on the free-surface of a precision-machined specimen plate, 2.5-cm thick, was plane parallel to the free surface within ±0.01μsec across an 8 to 10 cm central section. Two pyrolytic graphite specimens* were positioned within this section and arranged as shown below so that the shock wave pressure was incident normal on the original plane of deposition (C-axis) of one specimen and parallel to the plane of deposition in the other specimen (A-axis).

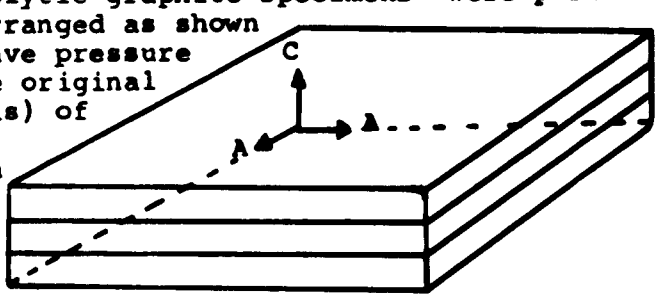


* The pyrolytic graphite, density 2.2 g/cm³, was obtained from High Temperatures Materials, Inc., Lowell, Mass.

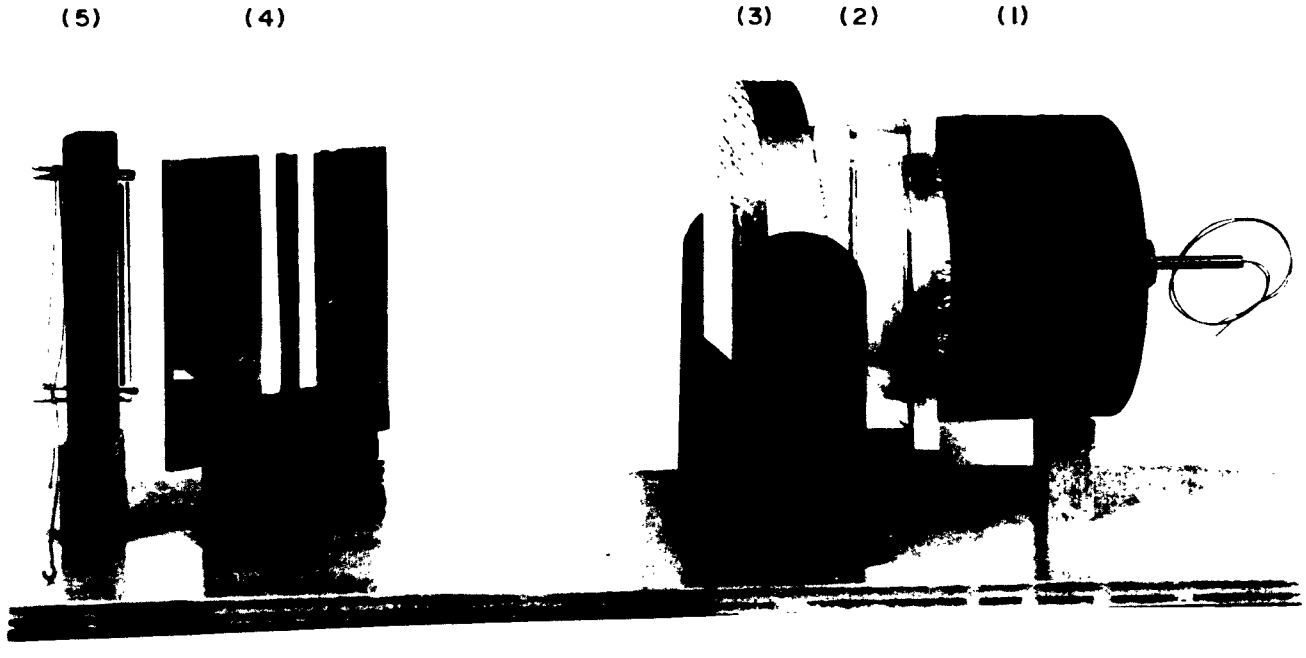


FIG. 1 EXPERIMENTAL ARRANGEMENT FOR DELIVERY OF A PLANE SHOCK WAVE TO THE TEST SPECIMENS. SHOWN ARE (1) THE PLANE-WAVE EXPLOSIVE LENS, (2) NITROMETHANE RESERVOIR, (3) SPECIMEN PLATE, (4) REFLECTED IMAGES OF THE TEST SPECIMENS, AND (5) THE EXPLODING-WIRE LIGHT SOURCES. OBSERVATIONS ARE MADE WITH A 2-SLIT, HIGH SPEED, ROTATING-MIRROR SMEAR CAMERA.

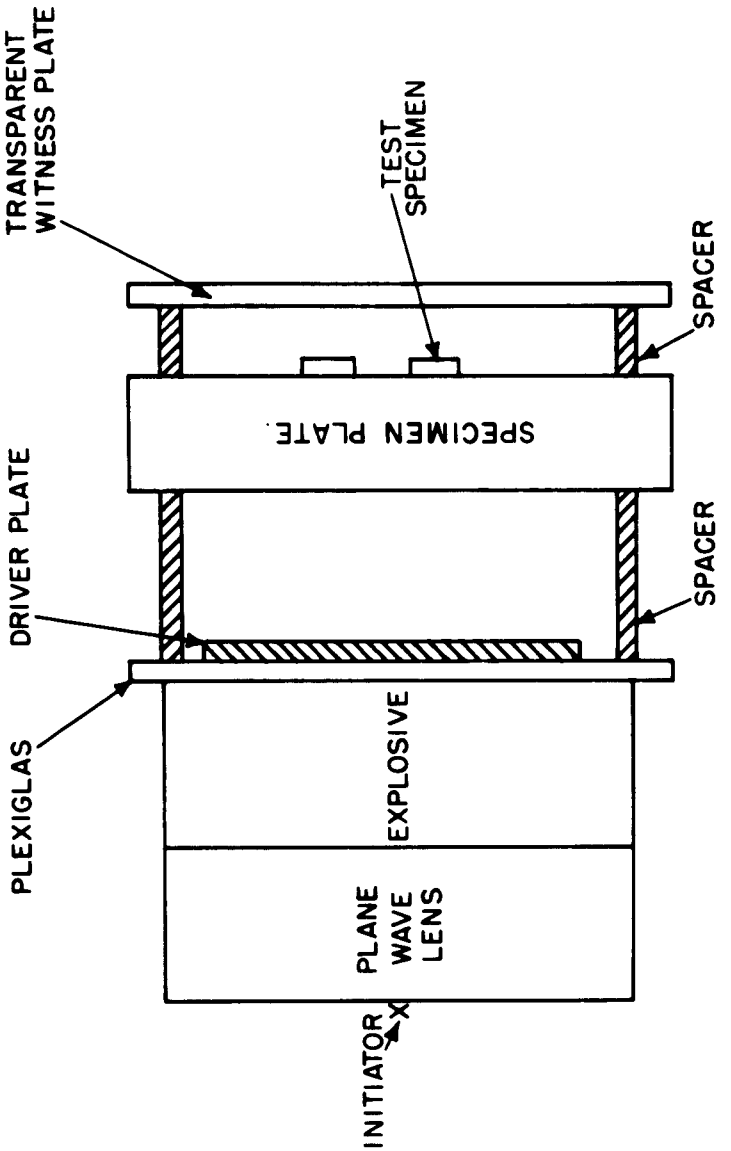


FIG. 2 ARRANGEMENT FOR OBTAINING PRESSURE OF 0.3-1.0 MEGABAR

In order to obtain an extensive range of data, it was necessary to produce in the specimens, shock waves of widely different fixed amplitudes, This was accomplished in three ways:

1. The shock pressure transmitted by the detonation of the explosive system was varied by using different explosive compositions. (In Fig. 1, the plane-wave generator ignited a liquid explosive, nitromethane, held in a Plexiglas shell.)

2. The shock from the explosive system was converted to a lower pressure by the impedance-mismatch method in which alternating layers of high and low density materials are utilized between the explosive and test specimens.

3. Higher shock pressures were produced by the free-run shots[10] in which the explosive system is used to propel a thin metal driver plate (Fig. 2) across an air gap of several centimeters into the back surface of the specimen plate.

The shock producing systems used in the experiments are given in Table 1.

The shock wave arrivals at the target plate and specimen free surfaces were recorded by a rotating mirror smear camera using a reflected light technique[12, 13, 14, 15]. In this method, light is reflected continuously from the free surfaces into the camera. Shock wave arrival at any point along the surface produces a sudden intensity change in light reflected from that point. This intensity change on shock wave arrival also signals the start of free surface motion. In the experimental arrangement shown in Fig. 1, light was provided by the explosion of two 0.0025-cm diameter, tungsten wires threaded into 10-cm long glass capillary tubes with an inside diameter of 0.1 cm. The wires were exploded 20 μsec. after initiation of the explosive system by discharging through them the energy from a 4 microfarad capacitor charged to 2000 volts. Light from the electrically-exploded wires passed through the cleared portions of the mirror to the specimen surfaces, (and the surface of the specimen plate), back to the mirror, where it was reflected to the smear camera. The free surfaces of the specimen and specimen plate were made reflective by attaching to them strips of aluminized mylar film. A thin film of lubricant was used to attach the film to the free surfaces. Reflected light from the shocked specimen plate arrangement, shown face-on to the shock in Fig. 3, was used to make the record shown in Fig. 4. As can be seen in Fig. 3, the left slit (No. 1) is looking directly at the test specimens and at the portions of the aluminum specimen plate which show between the test specimens. This arrangement shows up as nine horizontal bands on Fig. 4, each labeled as aluminum (specimen plate) or test

TABLE 1

EXPLOSIVE-GENERATED SHOCK SYSTEMS AND CALIBRATION PARAMETERS

| System No. | Explosive* Thick.(cm) | Shock-Driving System Thick.(cm) | Specimen Plate Thick.(cm) | | Pressure** (kb) | Particle** Velocity (mm/μsec) |
|---|---|---|---|---|---|---|
| 1 | 2.54 TNT | — | 1.27 | Brass | 202 | 0.530 |
| 2 | 2.54 TNT | — | 2.54 | Brass | 227 | 0.580 |
| 3 | 2.54 TNT | — | 1.27 | Brass | 240 | 0.613 |
| 4 | 2.54 TNT | 0.838 Brass/0.838 Plexiglas | 0.846 | Brass | 108 | 0.310 |
| 5 | 2.54 TNT | 1.27 Brass/1.27 Plexiglas | 1.27 | Brass | 95.4 | 0.279 |
| 6 | 2.54 TNT | 1.27 Plexiglas | 1.27 | Brass | — | — |
| 7 | 2.54 TNT | 0.254 Monel/1.91 Free Run | 0.787 | Al | 543 | 2.33 |
| 8 | 5.08 Comp B | — | 2.54 | Al | 254 | 1.30 |
| 9 | 5.08 Comp B | 0.152 Monel/1.27 Free Run | 0.914 | Brass | 752 | 1.50 |
| 10 | 3.75 $CH_3NO_3$ | — | 3.75 | Brass | 200 | 0.530 |
| 11 | 3.75 $CH_3NO_3$ | 0.254 Brass/1.27 Free Run | 1.27 | Brass | 566 | 1.19 |
| 12 | 3.75 $CH_3NO_3$ | — | 2.54 | Al | 206 | 1.08 |
| 13 | 3.75 $CH_3NO_3$ | 0.152 Monel/1.27 Free Run | 1.27 | Al | 318 | 1.55 |
| 14 | 3.75 $CH_3NO_3$ | 0.457 Steel/1.27 Free Run | 1.27 | Al | 356 | 1.69 |
| 15 | 3.75 $CH_3NO_3$ | 0.152 Monel/1.27 Free Run | 1.27 | Brass | — | — |

* 13.9 cm-diameter.

** Shock-wave parameters of specimen plate.

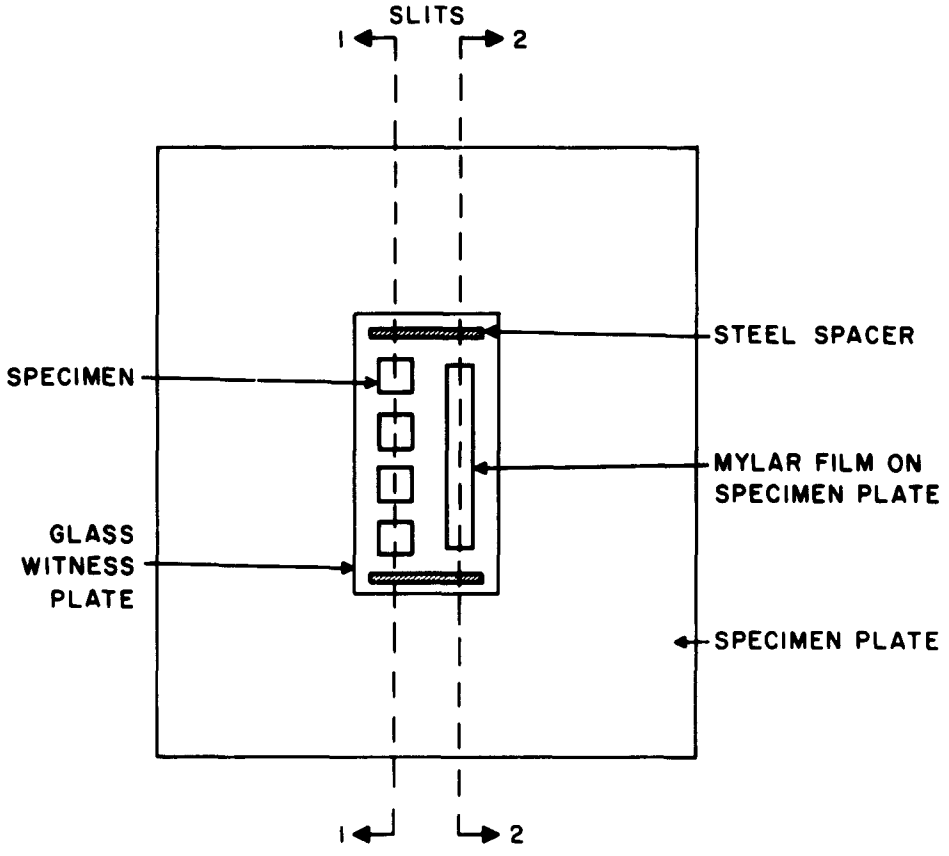


FIG. 3 SPECIMEN PLATE ARRANGEMENT

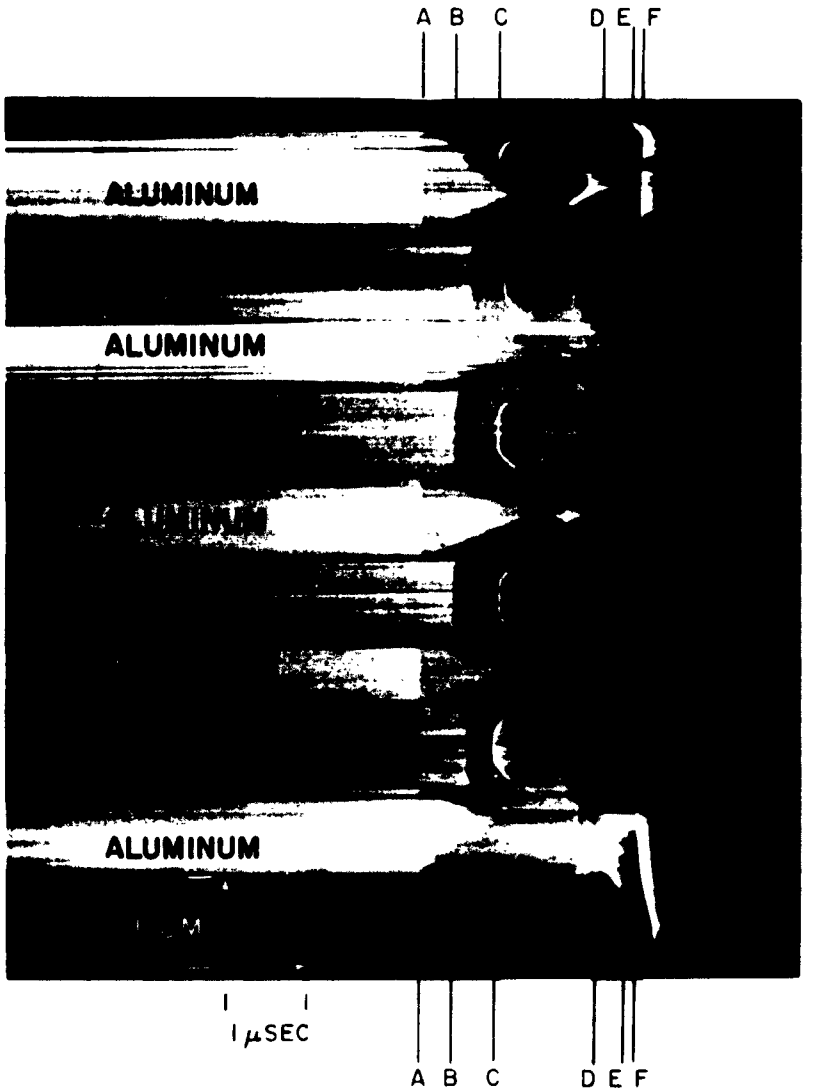


FIG. 4 TWO-SLIT SMEAR CAMERA RECORD OF SHOCK WAVE ARRIVALS ON THE FREE SURFACES OF THE TEST SPECIMENS AND ALUMINUM SPECIMEN PLATE, AND FREE-SURFACE ARRIVALS AT THE GLASS WITNESS PLATE

specimen (BN, PG #2, PG #1, Nylon). The right hand slit (No. 2) in Fig. 3 is aligned to look directly at the specimen plate which at this point is covered by a narrow strip of 0.015-mm thick mylar film.

As time goes from left to right on Fig. 4, there appear a sequence of six events, designated A through F. Event A, which shows as a darkening of the horizontal bands labeled aluminum, indicates the time at which the shock wave emerged from the aluminum specimen plate and entered the rear of each test specimen as seen by slit #1. Event D on these same bands is the same event in time as A except as viewed by slit 2*. Event B is the arrival of the shock at the front (or free surface) of the test specimens as viewed by slit #1. Event C is the arrival at the glass witness plate of the free surfaces of the test specimens, as viewed by slit #1. Event E, recorded by slit #2, indicates that the mylar film being driven toward the witness plate is compressing the intervening air to a state of shock luminosity. Although only faintly discernible, Event F, also recorded by slit #2, indicates the arrival of the free-surface of the aluminum at the glass witness plate. Calculation of the times of these events were then made as follows:

The horizontal displacement between Event B and Event A represents the shock wave transit time through the test specimen. (This displacement on the original film in millimeters divided by 3.8 gives the time in microseconds.) The mean shock wave velocity, of course, is determined by dividing the test specimen's thickness by this transit time.

Similarly the horizontal displacement between Events B and C is used to calculate the free-surface velocity of the test specimen. (In the measurement of Event C, the sharpest signal occurred at the first emittance of light from the shocked air layer in the gap and this was taken as indicating the arrival time although it obviously is indicating a somewhat too early time. The correction to the free-surface transit times is about 0.005 μsec and was obtained from reflected light experiments.)

The horizontal displacement between Events D and F permits calculation of the free-surface velocity of the aluminum specimen plate in a similar manner. The shock wave velocity corresponding to the free-surface velocity of the specimen plate material was calculated from its equation of state.

---

*When the shock arrives at each free surface, aluminum, specimen, or mylar, the camera image would be extinguished over the slit length viewing that surface and the traces would then go dark. However, because of the slits' displacement, light reflected from the mylar is still seen between Events A and D, and B and D. Actually, the sharp intensity changes at Event A and D occur simultaneously but are displaced on the record because of the slits' separation.

TABLE 2

SUMMARY OF SHOCK WAVE MEASUREMENTS
ALONG A AND C AXES

| System | Axis | Shock Velocity (mm/μsec) | Particle* Velocity (mm/μsec) | Particle** Velocity (mm/μsec) |
|---|---|---|---|---|
| 3 | C | 5.901 | 0.893 | 1.180 |
| 3 | C | 5.955 | 0.885 | 1.170 |
| 2 | C | 5.790 | 0.855 | 0.880 |
| 2 | A | 5.790 | 0.860 | 0.880 |
| 1 | A | 5.514 | 0.787 | 0.793 |
| 4 | C | 4.932 | 0.464 | —— |
| 4 | A | 4.932 | 0.464 | —— |
| 5 | A | 4.420 | 0.305 | —— |
| 5 | A | 4.420 | 0.305 | —— |
| 4 | A | 5.016 | 0.404 | —— |
| 4 | C | 5.003 | 0.479 | —— |
| 5 | C | 4.750 | 0.350 | —— |
| 6 | A | 5.750 | —— | 0.881 |
| 6 | C | 5.700 | —— | 0.884 |
| 10 | C | 5.440 | 0.798 | 0.834 |
| 10 | A | 5.440 | 0.802 | 0.880 |
| 8 | C | 6.550 | 1.504 | 1.398 |
| 8 | A | 6.617 | 1.487 | 1.393 |
| 12 | C | 6.337 | 1.237 | 1.287 |
| 12 | A | 6.284 | 1.239 | 1.306 |
| 9 | C | 7.803 | 2.252 | 2.328 |
| 13 | C | 8.370 | —— | 2.516 |
| 7 | C | 8.342 | 2.501 | 2.490 |
| 14 | C | 7.445 | 1.900 | —— |
| 11 | C | 7.628 | 2.180 | —— |
| 13 | A | 8.322 | 2.332 | 2.390 |
| 15 | A | 7.577 | —— | 2.059 |

* Impedance-match calculation
** Free-surface velocity approximation

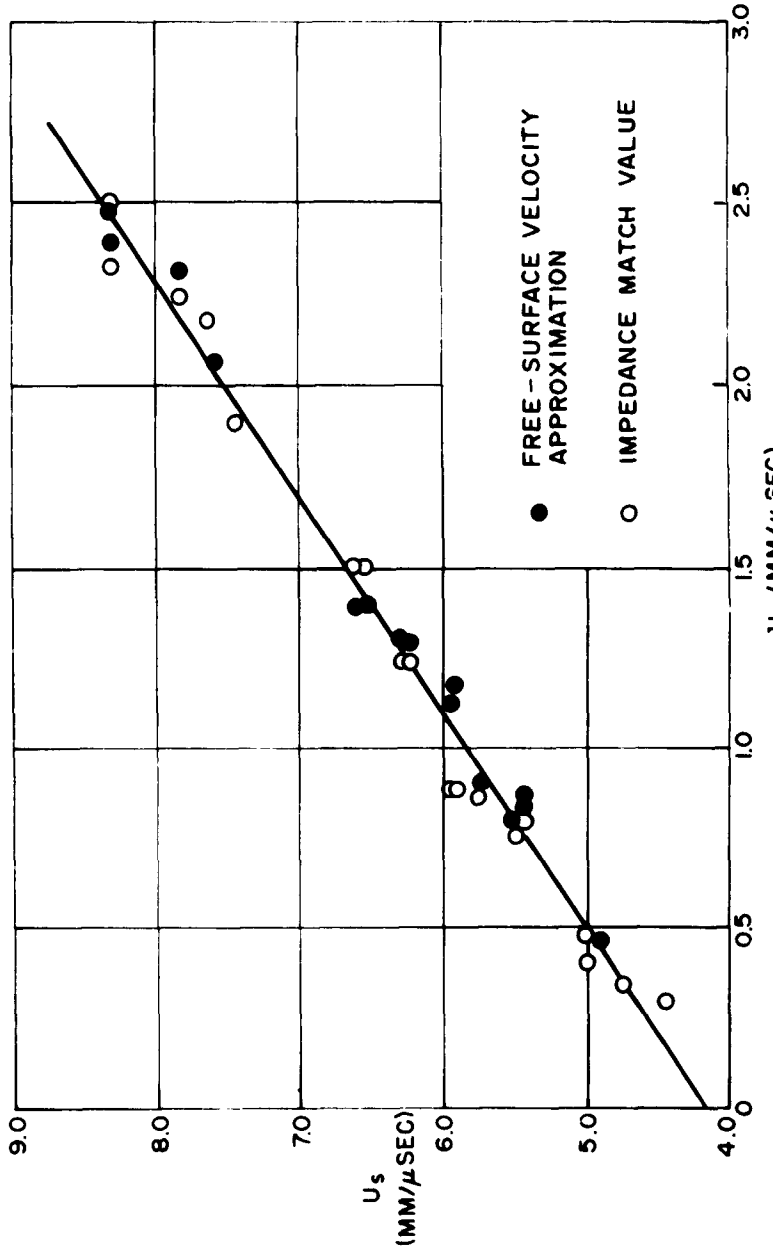


FIG. 5 SHOCK VELOCITY ($U_s$) – PARTICLE VELOCITY ($U_p$) CURVE FOR PYROLYTIC GRAPHITE

## IV. RESULTS

The experimental measurements of the shock wave and particle velocities are listed in Table 2 and plotted in Fig. 5. Particle velocities determined using the impedance-matching method and the free-surface velocity approximation are identified in Table 2 and Fig. 5. Shock wave and particle velocities measured along the C and A axes are identified only in Table 2. Velocity differences exceeding experimental errors were not noted between the shock wave parameters measured along either orientation. Therefore the data points were not differentiated in regard to orientation in Fig. 5.

The Rankine-Hugoniot values of pressure and specific volume calculated using the least square measurements of $U_s$ and $u_p$ ($U_s$=4.149 + 1.690 $u_p$) (mm/μsec) are listed in Table 3 and plotted in Fig. 6. The compressibility coefficient, $(1/V_o)$ $(\Delta V/\Delta P)$, computed from differences in the decrease of specific volume for increasing pressure are plotted against the relative volume, $(V_o-V)/V_o$, in Fig. 7.

The errors in the experimental measurements of the shock velocity and particle velocity resulted from uncertainties in machining the pellets, in mounting the witness plates for free-surface velocity measurements, in shock wave curvature and in record analysis. The root-mean-square error of ± 100 m/sec in $U_s$ and ± 92 m/sec in $u_p$, lead to relative errors of ± 2 per cent in specific volume and ± 7 per cent in pressure (at 200 kb) when the graphite was compressed to 80 per cent of its original volume.

## V. DISCUSSION

The straight line plot of Fig. 5 is typical of the shock velocity-particle velocity relationship for many solids, and therefore is useful for the study of shock-induced phase transitions. If the transformation of pyrolytic graphite to diamond occurred within this compression range, the shock velocity-particle velocity co-ordinates for each phase would lie on a separate line each given by a different slope. This trend is not obtained from the data plotted in Fig. 5.

Although the shock wave measurements failed to distinguish between the two orientations in regard to their dynamic compression characteristics, measurements of the sound velocity showed considerable anisotropy. Experimental determinations (Table 4) of the longitudinal sound velocity were made as a function of temperature from 0°C to 100°C using an ultrasonic method[18]. At 20°C, the velocity in the C-direction was 2930 m/sec and in the A-direction 4550 m/sec. The velocity measured in the C-direction increased by 285 m/sec when the temperature of the test specimen was raised from 0°C to 100°C. A slight decrease of 28 m/sec was measured in the A-direction over the same temperature range.

TABLE 3

RANKINE-HUGONIOT SHOCK WAVE PARAMETERS
OF PYROLYTIC GRAPHITE

| $U_s$ mm/μsec | $u_p$ mm/μsec | P (kb) | V $cm^3/g$ |
|---|---|---|---|
| 4.149 | 0 | 0 | .4545 |
| 4.487 | 0.200 | 19.74 | .4342 |
| 4.825 | 0.400 | 42.46 | .4168 |
| 5.163 | 0.600 | 68.15 | .4017 |
| 5.501 | 0.800 | 96.82 | .3884 |
| 5.839 | 1.000 | 128.5 | .3766 |
| 6.177 | 1.200 | 163.1 | .3662 |
| 6.515 | 1.400 | 200.7 | .3568 |
| 6.853 | 1.600 | 241.2 | .3484 |
| 7.191 | 1.800 | 284.8 | .3407 |
| 7.529 | 2.000 | 331.3 | .3338 |
| 7.867 | 2.200 | 380.8 | .3274 |
| 8.205 | 2.400 | 433.2 | .3216 |
| 8.543 | 2.600 | 488.7 | .3162 |

TABLE 4

LONGITUDINAL SOUND VELOCITY

| C-AXIS | | A-AXIS | |
|---|---|---|---|
| Temp. (°C) | Velocity (mm/μsec) | Temp. (°C) | Velocity (mm/μsec) |
| 0.75 | 2.867 | 0.20 | 4.558 |
| 10.0 | 2.887 | 10.1 | 4.556 |
| 21.8 | 2.933 | 20.1 | 4.555 |
| 30.2 | 2.963 | 30.0 | 4.551 |
| 39.6 | 2.973 | 40.0 | 4.547 |
| 50.6 | 3.029 | 50.2 | 4.543 |
| 60.0 | 3.048 | 60.0 | 4.541 |
| 70.0 | 3.078 | 70.8 | 4.536 |
| 79.9 | 3.107 | 80.3 | 4.534 |
| 90.0 | 3.133 | 89.6 | 4.531 |
| 98.6 | 3.152 | 99.0 | 4.530 |

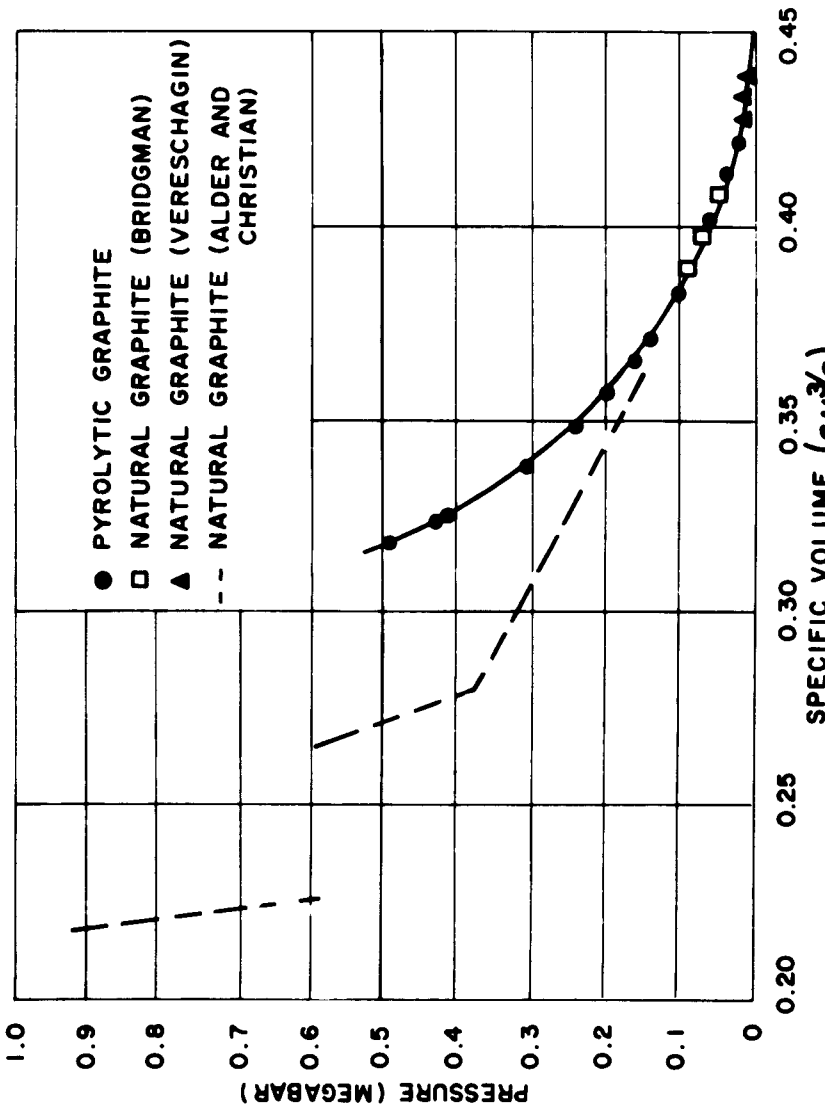


FIG. 6 THE COMPRESSIBILITY OF GRAPHITE

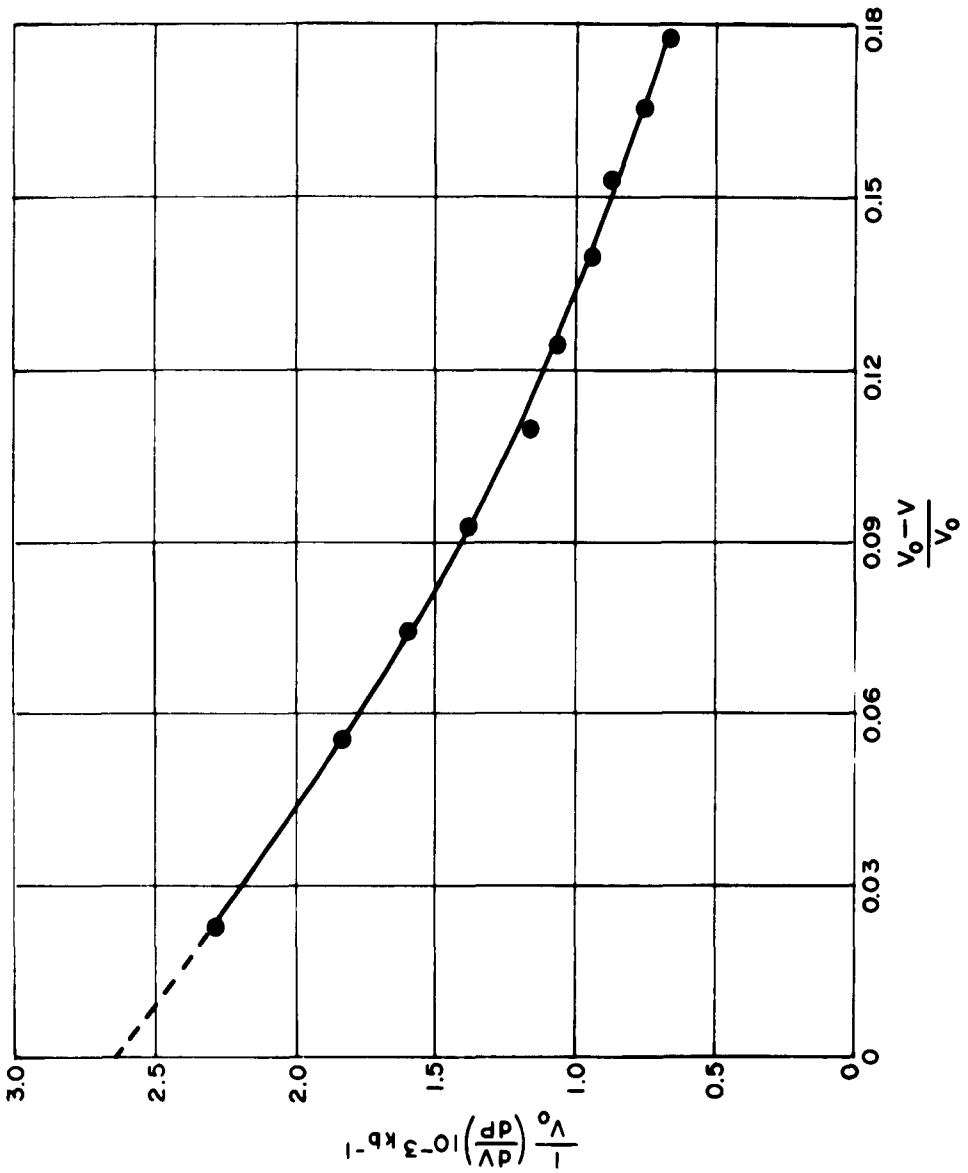


FIG. 7 COMPRESSIBILITY VS RELATIVE VOLUME OF PYROLYTIC GRAPHITE

The data of Fig. 7 show that the compressibility of pyrolytic graphite drops rapidly with increasing pressure; the bulk modulus decreases by 50 per cent when the relative compression is increased from 0.08 (40 kilobars) to 0.13 (80 kilobars). An extrapolation of the data to P=0, yields the initial compressibility, $1/V_0$ (dV/dP) of pyrolytic graphite as $2.64 \times 10^{-12}$ cm²/dyne. This number is about 10 per cent less than the static isothermal compressibility value ($3.0 \times 10^{-12}$ cm²/dyne) measured by Bridgman[6] and Richards[17] for natural graphite, and is in close agreement with the value ($2.56 \times 10^{-12}$ cm²/dyne) calculated by Brennan[18] from quantum considerations of the graphite lattice.

The Rankine-Hugoniot measurements for pyrolytic graphite in Fig. 6 differ significantly from the measurements of Alder and Christian for natural graphite from Ceylon. These authors interpreted the upper line drawn through their data as resulting from the conversion of the solid to a closely-packed metallic liquid, and the lower curve beginning at 0.4 megabar to nearly complete conversion of graphite to diamond. The pyrolytic graphite, P-V curve, up to 0.5 megabar, however, is well-behaved, and no phase transformations are indicated.

A plausible explanation of the difference in the equations of state may be developed from the studies of Samara and Drickamer[8] and Bundy[19] on the resistance vs static pressure behavior of pyrolytic graphite. At low pressures, the resistance of pyrolytic graphite along its C-axis is nearly 20 times that of random polycrystalline graphites. Pyrolytic graphite has a sharper decrease in the slope of its resistance-pressure curve; its resistance at 130 kb is 7 times greater than polycrystalline graphite. These data indicate that the compressibility of pyrolytic graphite decreases more rapidly at high pressures.

The presence of structural impurities in Ceylon graphite is also a possible explanation of the difference in the P-V data for pyrolytic graphite and natural Ceylon graphite. In 1942 Lipson and Stokes[20] reported the existence of 14 per cent of the rhombohedral structure in natural graphite from Ceylon. De Carlie and Jamieson suggest the transformation under shock compression of regions having the rhombohedral structure as the probable origin of the diamonds in their recovered specimens. Although under dynamic (shock wave) compression pyrolytic graphite behaves similar to pure hexagonal graphite, from which diamonds have not been produced by shock wave compression, Bundy has recovered diamonds from a pyrolytic graphite specimen that was statically-compressed to 130 kb. In Bundy's experiments, in order for the transformation to occur, it was necessary to heat the sample to a temperature above 3000°C during the compression. It is of interest, therefore, to calculate the temperatures associated with the shock wave compression of pyrolytic graphite. These temperatures can be calculated[9, 21] by combining the various thermodynamic relations with the Rankine-Hugoniot equation:

$$E - E_0 = 1/2\ (P + P_0)\ (V_0 - V) \qquad (4)$$

to obtain the increase in specific energy of material at the shock front as a function of pressure and volume. The solution of equation (4) gives a P-V curve (dynamic adiabat) of the same form as an isotherm. Since temperature changes can be expected to have only a small effect on the compressibility of graphite, related adiabats and isotherms then can be determined from the known Rankine-Hugoniot P-V data and temperatures, using the second law of thermodynamics. The results of these calculations (Table 5) show that for a shock pressure of 128 kilobars, the calculated temperature rise in the compressed pyrolytic graphite is only 189°K, and even when the material is compressed by 490 kilobars the temperature rise of 2100°K is still surprisingly low. Since in these experiments the duration of shock pressure was less than 1μsec and the temperatures due to the shock wave compression were low, much higher dynamic pressures would have to be utilized for a direct transition of pyrolytic graphite to diamond.

TABLE 5

CALCULATED RANKINE-HUGONIOT TEMPERATURES AND 25°C ISOTHERM FOR THE COMPRESSION OF PYROLYTIC GRAPHITE

| V $cm^3/g$ | $T_{(R-H)}$ (°K) | $P_{(R-H)}$ (kb) | $P_I$ (kb) |
|---|---|---|---|
| 0.4545 | 298 | 0 | 0 |
| 0.4250 | 314 | 30.3 | 30.2 |
| 0.4014 | 354 | 67.5 | 67.0 |
| 0.3945 | 378 | 81.5 | 80.8 |
| 0.3882 | 407 | 96.2 | 95.3 |
| 0.3764 | 487 | 128 | 127 |
| 0.3714 | 535 | 145 | 143 |
| 0.3577 | 725 | 202 | 198 |
| 0.3486 | 932 | 241 | 236 |
| 0.3382 | 1247 | 310 | 302 |
| 0.3314 | 1541 | 359 | 349 |
| 0.3259 | 1840 | 410 | 397 |
| 0.3227 | 2045 | 438 | 423 |
| 0.3177 | 2461 | 494 | 476 |

## VI. REFERENCES

1. B. J. Alder and R. H. Christian, Phys. Rev. Letters, 7, 367 (1961).
2. P. S. De Carlie and J. C. Jamieson, Science, 133, 1821 (1961).
3. K. Komatsu, J. Phys. Chem. Solids, 6, 380 (1958).
4. G. A. Stack, Bull. Am. Phys. Soc., 7, 192 (1962).
5. G. A. Samara and H. G. Drickamer, J. Chem. Phys. 37, 471 (1962).
6. P. W. Bridgman, Proc. Am. Acad. Arts and Sci., 76, 55 (1948).
7. L. F. Vereschagin, Processes in Very High Pressure Research (John Wiley and Sons, Inc., New York, 1961) p. 290.
8. R. W. Goranson, D. Bancroft, B. L. Burton, T. Blechar, E. E. Houston, E. F. Gittings, and S. A. Landeen, Appl. Phys., 26, 1472 (1955).
9. J. M. Walsh and R. H. Christian, Phys. Rev. 97, 1544 (1955).
10. R. G. McQueen and S. P. Marsh, J. Appl. Phys.,31, 1253 (1960).
11. J. H. Cook, Research (London), 1, 474 (1948).
12. T. P. Cotter, Thesis, Cornell University (1953).
13. W. A. Allen and C. L. McGary, Rev. Sci. Inst., 29, 165 (1953).
14. N. L. Coleburn, NAVORD Report 6026 (1960).
15. T. P. Liddiard and B. E. Drimmer, J. SMPTE, 70 (1961).
16. H. T. Savage, Naval Ordnance Laboratory, Personal Communication.
17. T. W. Richard, Zeit Elektrochem 13, 519 (1907).
18. R. O. Brennan, J. Chem. Phys., 20, 40 (1951).
19. F. P. Bundy, J. Chem. Phy., 38, 631 (1963).
20. H. Lipson and A. R. Stokes, Proc. Roy. Soc. (London), 181, 101 (1942).
21. J. Wacherle, J. Appl. Phys., 33, 922 (1962).

DISTRIBUTION

| | Copies |
|---|---|
| Chief, Bureau of Naval Weapons<br>Navy Department<br>Washington 25, D. C. | |
| DLI-3 | 1 |
| RM | 1 |
| RMMP-21 | 1 |
| RMMO-212 | 1 |
| RMGA-534 | 1 |
| RRRE-6 | 1 |
| Dr. Land, RUME-11 | 1 |
| Mr. E. Fisher, RMMO-13 | 1 |
| Mr. G. Edwards, RUME-33 | 1 |
| Mr. W. August, RRRE-51 | 1 |
| RMMO-5 | 1 |
| RUME-32 | 1 |
| Director, Special Projects Office<br>Department of the Navy<br>Washington 25, D. C. | |
| SP-1142 | 1 |
| Office of Naval Research<br>Department of the Navy<br>Washington 25, D. C. | |
| Power Branch, Code 429 | 1 |
| Material Branch | 1 |
| Commander<br>U. S. Naval Ordnance Test Station<br>China Lake, California | |
| Code 556 | 1 |
| Code 4572 | 1 |
| Technical Library | 2 |
| H. Dean Mallory | 1 |
| R. Plauson | 1 |
| Director, Naval Research Laboratory<br>Department of the Navy<br>Washington 25, D. C. | 1 |
| Commander<br>U. S. Naval Weapons Laboratory<br>Dahlgren, Virginia | |
| Technical Library | 2 |
| Weapons Lab. | 1 |
| Terminal Ballistics Lab. | 1 |
| Commanding Officer<br>U. S. Naval Weapons Station<br>Yorktown, Virginia | |
| R&D Division | 2 |
| Commandant, U. S. Marine Corps.<br>Washington 25, D. C. | 1 |

| | Copies |
|---|---|
| Commanding Officer<br>U .S. Naval Ordnance Laboratory<br>Corona, California | 1 |
| Commanding Officer<br>U. S. Naval Weapons Evaluation Facility<br>Kirtland Air Force Base<br>Albuquerque, New Mexico | 1 |
| Commanding Officer<br>U. S. Naval Propellant Plant<br>Indian Head, Maryland | |
| Technical Library | 1 |
| EODTC | 1 |
| Commanding General<br>Aberdeen Proving Ground<br>Aberdeen, Maryland | |
| Technical Library | 1 |
| Dr. R. Eichelberger | 1 |
| Army Material Command<br>Department of the Army<br>Washington 25, D. C. | |
| R&D Division | 1 |
| Commanding Officer<br>U. S. Army<br>Engineer R&D Laboratory<br>Ft. Belvoir, Virginia | |
| Tech. Intelligence Branch | 1 |
| Commanding General<br>Redstone Arsenal<br>Huntsville, Alabama | |
| Technical Library | 1 |
| Office of Chief of Engineers<br>Department of the Army<br>Washington 25, D. C. | |
| ENGNB | 1 |
| ENGEB | 1 |
| Commanding Officer<br>Picatinny Arsenal<br>Dover, New Jersey | |
| ORDBB-TH8 | 1 |
| ORDBB-TJ1 | 1 |
| ORDBB-TK3 | 1 |
| ORDBB-TM1 | 1 |
| ORDBB-TP1 | 1 |
| ORDBB-TP2 | 1 |
| ORDBB-TP3 | 2 |
| ORDBB-TR2 | 1 |
| ORDBB-TS1 | 1 |

| | Copies |
|---|---|
| Commanding Officer<br>Harry Diamond Laboratories<br>Connecticut Ave. & Van Ness St., N. W.<br>Washington 25, D. C. | |
| Ord. Development Lab. | 1 |
| M. Lipnick, Code 005 | 1 |
| J. Hershkowitz | 1 |
| Chief of Staff<br>U. S. Air Force<br>Washington 25, D. C. | |
| AFORD-AR | 1 |
| APGC (PGTRI Tech. Lib.)<br>Eglin Air Force Base, Florida | 1 |
| Office of Technical Services<br>Department of Commerce<br>Washington 25, D. C. | 100 |
| Defense Documentation Center<br>Arlington Hall Station<br>Arlington 12, Virginia | |
| TIPCR | 10 |
| Chief<br>Defense Atomic Support Agency<br>Washington 25, D. C. | 5 |
| Atomic Energy Commission<br>Washington 25, D. C. | |
| DMA | 1 |
| Sandia Corporation<br>P. O. Box 5400<br>Albuquerque, New Mexico | |
| J. Weber | 1 |
| Director, Applied Physics Laboratory<br>Johns Hopkins University<br>8621 Georgia Avenue<br>Silver Spring, Md. | 1 |
| New Mexico Institute of Mining and Technology<br>Socorro, New Mexico | 1 |
| Director, U. S. Bureau of Mines<br>Division of Explosive Technology<br>4800 Forbes Street<br>Pittsburgh 13, Pennsylvania | |
| Dr. R. W. Van Dolah | 1 |

| | Copies |
|---|---|
| Headquarters<br>National Aeronautics & Space Administration<br>1520 H Street, N. W.<br>Washington 25, D. C. | 1 |
| National Aeronautics & Space Administration<br>Goddard Space Flight Center<br>Greenbelt, Maryland | 1 |
| Lewis Research Center, NASA<br>21000 Brookpark Road<br>Cleveland 35, Ohio<br>Library | 1 |
| Ames Research Laboratory, NASA<br>Moffett Field, California | 1 |
| Armed Services Explosives Safety Board<br>Building T-7 Gravelly Point<br>Washington, D. C. | 1 |
| Director, Office of the Secretary of Defense<br>Adv. Res. Projects Agency<br>Washington 25, D. C.<br>Dr. John F. Kincaid | 1 |
| Los Alamos Scientific Laboratory<br>P. O. Box 1663, Los Alamos, New Mexico<br>Dr. L. C. Smith | 1 |
| University of Utah<br>Salt Lake City, Utah<br>Dr. M. Cook | 1 |
| Arenberg Ultrasonics Laboratory<br>94 Green Street<br>Jamaica Plain 30, Massachusetts<br>D. L. Arenberg | 1 |
| Lawrence Radiation Laboratory<br>University of California<br>P. O. Box 808<br>Livermore, California | |
| Tech. Information Division | 1 |
| Dr. M. Wilkins | 1 |
| Dr. J. Kurry | 1 |
| Aerojet-General Corp.<br>1711 Woodruff Avenue<br>Downey, California<br>Dr. L. Zernow | 1 |

| | Copies |
|---|---|
| Aerojet-General Corp.<br>P. O. Box 1168<br>Sacramento, California<br>Dr. W. Kirchner | 1 |
| Bureau of Naval Weapons Representative<br>(Special Projects Office)<br>Lockheed Missiles and Space Co.<br>P. O. Box 504<br>Sunnyvale, California<br>SPL-313 | 2 |
| Bureau of Naval Weapons Resident Representative<br>(Special Projects Office)<br>Aerojet-General Corp.<br>Sacramento, California<br>SPLA-30 | 1 |
| Bureau of Naval Weapons Representative<br>Allegheny Ballistics Laboratory<br>Cumberland, Maryland<br>SPH-30 | 1 |
| Allegheny Ballistics Laboratory<br>Hercules Powder Co.<br>Cumberland, Md.<br>Dr. N. F. LeBlanc<br>Mr. R. Richardson | 1<br>1 |
| Aeronutronics<br>A Division of Ford Motor Co.<br>Ford Road<br>Newport Beach, California<br>Mr. S. Weller<br>Mr. M. Boyer | 1<br>1 |
| Rohm and Haas Co.<br>Redstone Arsenal<br>Huntsville, Alabama<br>Dr. H. Shuey | 1 |
| Space Technology Laboratory<br>P. O. Box 95001<br>Los Angeles 45, California<br>Mr. H. A. Taylor<br>VIA: Navy Liaison Office (SP)<br>AFU P. O. Los Angeles, Calif.<br>M. H. Holt | 1<br>1 |

CATALOGING INFORMATION FOR LIBRARY USE

BIBLIOGRAPHIC INFORMATION

| | DESCRIPTORS | CODES | | DESCRIPTORS | CODES |
|---|---|---|---|---|---|
| SOURCE | NOL technical report | NOLTR | SECURITY CLASSIFICATION AND CODE COUNT | Unclassified - 25 | UØ25 |
| REPORT NUMBER | 63-73 | 63ØØ73 | CIRCULATION LIMITATION | | |
| REPORT DATE | 22 May 1963 | Ø563 | CIRCULATION LIMITATION OR BIBLIOGRAPHIC | | |
| | | | BIBLIOGRAPHIC (SUPPL., VOL., ETC.) | | |

SUBJECT ANALYSIS OF REPORT

| DESCRIPTORS | CODES | DESCRIPTORS | CODES | DESCRIPTORS | CODES |
|---|---|---|---|---|---|
| Compressibility | COMR | Plane | PLNE | Transition | TRNI |
| Pyrolytic | PYRL | Deposition | DEPS | | |
| Graphite | GRAP | Optical | OPTI | | |
| Measurement | MEAU | Rankine | RANK | | |
| Explosive | EXPL | Hugoniot | HUGO | | |
| Generated | GENO | Equations | EQUA | | |
| Shock waves | SHWV | Points | POIN | | |
| Shock | SHOC | Crystal | CRYS | | |
| Surface | SURA | Directions | DIRC | | |
| Velocities | VELC | Pressure | PRES | | |
| Normal | NORM | Volume | VOLU | | |
| Parallel | PALE | Diamond | DIAO | | |

Naval Ordnance Laboratory, White Oak, Md.
(NOL technical report 63-73)
THE COMPRESSIBILITY OF PYROLYTIC GRAPHITE, by N. L. Coleburn. 22 May 1963. 20p. illus. tables. UNCLASSIFIED

The compressibility of pyrolytic graphite has been dynamically measured at pressures up to 0.5 megabar by utilizing explosive-generated shock waves. At pressures above 100 kilobars the results differ significantly from those obtained by Alder and Christian on natural graphite from Ceylon. Within the range of the present experiments no transition of pyrolytic graphite to diamond was found.

1. Graphite, Pyrolytic
2. Graphite - High pressure
3. Graphite - Compressibility
I. Title
II. Coleburn, Nathaniel L.

Naval Ordnance Laboratory, White Oak, Md.
(NOL technical report 63-73)
THE COMPRESSIBILITY OF PYROLYTIC GRAPHITE, by N. L. Coleburn. 22 May 1963. 20p. illus. tables. UNCLASSIFIED

The compressibility of pyrolytic graphite has been dynamically measured at pressures up to 0.5 megabar by utilizing explosive-generated shock waves. At pressures above 100 kilobars the results differ significantly from those obtained by Alder and Christian on natural graphite from Ceylon. Within the range of the present experiments no transition of pyrolytic graphite to diamond was found.

1. Graphite, Pyrolytic
2. Graphite - High pressure
3. Graphite - Compressibility
I. Title
II. Coleburn, Nathaniel L.

Naval Ordnance Laboratory, White Oak, Md.
(NOL technical report 63-73)
THE COMPRESSIBILITY OF PYROLYTIC GRAPHITE, by N. L. Coleburn. 22 May 1963. 20p. illus. tables. UNCLASSIFIED

The compressibility of pyrolytic graphite has been dynamically measured at pressures up to 0.5 megabar by utilizing explosive-generated shock waves. At pressures above 100 kilobars the results differ significantly from those obtained by Alder and Christian on natural graphite from Ceylon. Within the range of the present experiments no transition of pyrolytic graphite to diamond was found.

1. Graphite, Pyrolytic
2. Graphite - High pressure
3. Graphite - Compressibility
I. Title
II. Coleburn, Nathaniel L.

Naval Ordnance Laboratory, White Oak, Md.
(NOL technical report 63-73)
THE COMPRESSIBILITY OF PYROLYTIC GRAPHITE, by N. L. Coleburn. 22 May 1963. 20p. illus. tables. UNCLASSIFIED

The compressibility of pyrolytic graphite has been dynamically measured at pressures up to 0.5 megabar by utilizing explosive-generated shock waves. At pressures above 100 kilobars the results differ significantly from those obtained by Alder and Christian on natural graphite from Ceylon. Within the range of the present experiments no transition of pyrolytic graphite to diamond was found.

1. Graphite, Pyrolytic
2. Graphite - High pressure
3. Graphite - Compressibility
I. Title
II. Coleburn, Nathaniel L.